Structural Correction of a Spherical Near-Field Scanner for mm-Wave Applications

Daniël Janse van Rensburg & Pieter Betjes
Nearfield Systems Inc.
19730 Magellan Drive
Torrance, CA
90502-1104, USA

***Abstract*— A spherical near-field test system allowing for the antenna under test to remain stationary during testing is described. The system is suitable for use at mm-wave (> 50 GHz) frequencies. Fidelity of the structure for testing at these frequencies is critical and since the structure experiences a gravitational force as a function of probe position, a complex deformation map results. There is also a radial distance variation of the probe and a technique to correct for this variation (presented before) is expounded upon. We describe the structural perturbation observed on such a scanner and assess to what extent this limits high frequency application for spherical near-field testing.**

I. INTRODUCTION

On-chip antenna innovation at mm-wave frequencies have led to the development of spherical near-field test systems that allow the antenna to remain stationary [1, 2]. These test systems, although simple conceptually, introduce very unique and challenging mechanical constraints. The system described here consists of a dual rotary stage articulating arm [3, p. 299] that moves the near-field probe on a spherical surface enclosing the antenna under test (AUT). In [1] the design of this system as well as simulations conducted to assess the design specifications was described. In [2] we reported initial spherical near-field test data as well as the pivotal radial correction technique. In this publication we provide detailed information on the measured structural performance of the scanner and discuss its suitability for spherical near-field (SNF) and far-field (FF) testing.

The articulating arm structure experiences the gravitational force as a function of SNF probe position, resulting in structural deformation which is variable. This deformation introduces radial distance variation of the probe and unwanted cross-coupling between the SNF position variables. This effect perturbs the ideal spherical surface that is assumed.

In Section II we define the coordinate system of the scanner and describe the structural perturbation observed. An interpretation of the data is presented in Section III in order to gain insight into the forces affecting the structure. In Section IV we address structural correction that can be considered and in Section V we outline to what extent this limits high frequency application for SNF testing. RF test data is presented in Section IV and the impact of radial distance correction is shown.

We conclude with general statements about SNF versus FF testing at mm-wave frequencies.

II. SPHERICAL COORDINATE SYSTEM IMPLEMENTATION

The coordinate system we are trying to emulate is that shown in Figure 1. The SNF scanner of interest is that illustrated in Figure 2. The large ϕ rotation stage rotates both articulating arms around the horizontal ϕ-axis as shown. The position shown in Figure 2 is $\phi = 0°$ and clock-wise rotation (facing the SNF probe) represents positive rotation angles.

The smaller θ rotation stage rotates the second articulating arm around the θ - axis as shown. It is important to note that although this axis is shown vertically in Figure 2, it varies with the ϕ variable. The arm position shown in Figure 2 is $\theta = 0°$ and clock-wise rotation (facing the θ stage) represents positive angles.

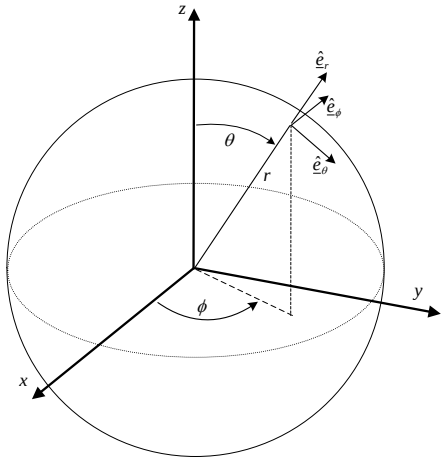

Figure 1. Spherical near-field coordinate system being implemented.

Also shown in Figure 2 is the polarization axis of rotation, indicated by variable χ.

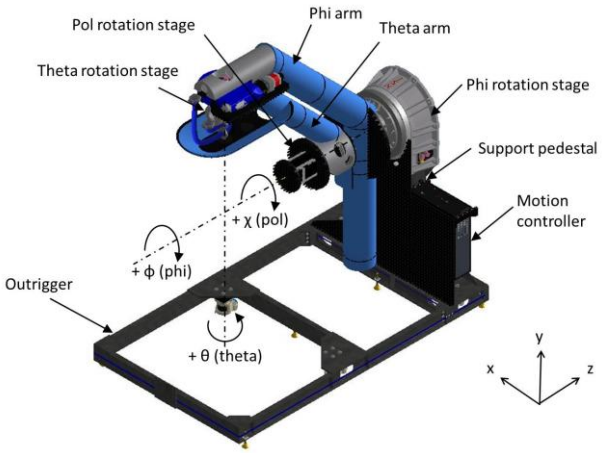

Figure 2. Schematic representation of an NSI-700S-360 articulated spherical near-field antenna test system showing the associated spherical measurement system axes.

Figure 3 depicts two distinct probe locations in order to illustrate the angular rotation conventions. It is important to also note that although the spherical coordinate system in Figure 1 only allows for positive angles of rotation, it is common practice in the antenna test community to allow negative angles of rotation as depicted here. The reason for this is to allow for continuous mechanical motion of the SNF probe across the poles of the sphere without requiring reversal of the ϕ - axis.

Figure 3. Two distinct probe positions are depicted. Top: θ = 135° & ϕ = 0°. Bottom: θ = 135° & ϕ = -90° = 270°.

Another benefit of allowing negative angles of rotation is that all probe positions can be achieved by two distinct angular settings (eg. θ = 90° and ϕ = 0° locates the probe in exactly the same position as θ = -90° and ϕ = 180°, barring a 180° polarization rotation of the probe) of the spherical variables. The significance of this is that the structural deformation for these two cases is different. Since the arms are subject to gravity in two different positions, comparing measurements made on these two alternate spheres allow for assessment of the impact of this deformation on electrical measurements.

III. Scanner Structural Assessment

Scanner structural and positioning performance data can be obtained from laser tracker dimensional measurements. These results allow one to establish a perturbed (θ', ϕ', r') grid, based on a regular (θ, ϕ, r) SNF grid. The structural deformation assessment by using a laser tracker is depicted in Figure 4. Due to visual blockage of the structure only a portion ($-110° \leq \theta \leq +110°$) of the sphere can be measured. The data measured for the three spherical variables (θ', ϕ', r') are compared to (θ, ϕ, r) to assess effective errors. Typical results are presented in Figures 5 – 7 below. Figure 5 shows radial distance error (variable $r' - r$) in mm as a function of variable ϕ for seven distinct values of variable θ. The curve depicting $\theta = 0°$ (solid curve without any designated symbol) represents the polar case where the SNF probe is ideally located in one position and simply rotates its polarization angle as a function of rotation in ϕ. However, instead of observing a fixed zero error we observe a variation that approximates a cosinusoidal curve with peak-to-peak amplitude of ± 0.3 mm. This behavior is a direct consequence of structural deformation of the arms as well as the θ and ϕ rotary stages due to gravity. A finite element analysis of this structure was presented in [1] and further insight into the structural behavior can be gained from the images presented there.

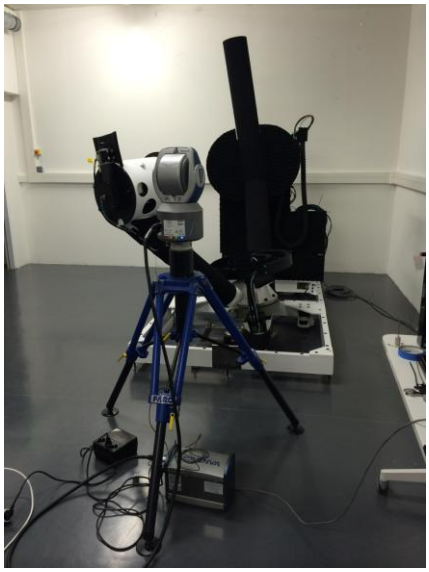

Figure 4. Structural measurement using a laser tracker. Note that only a portion of the full spherical surface can be evaluated.

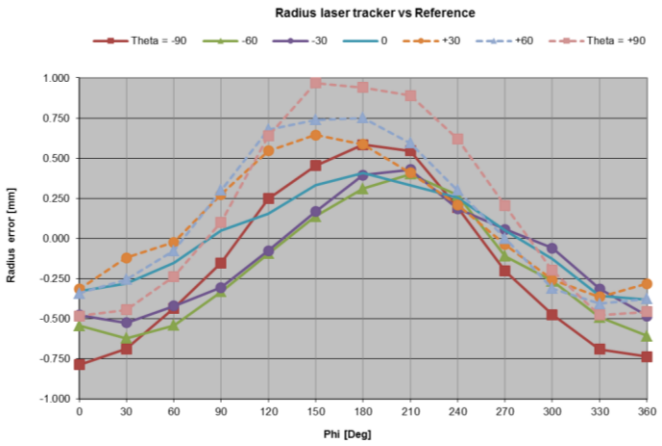

Figure 5. Strucural laser tracker measurement showing *r'* error as a function of ϕ variable. Curves represent discrete values of θ variable.

Also noteworthy in Figure 5 are the two curves depicting θ = ±90° (solid and dashed curves with ■ symbol). These two cases represent the equatorial motion of the SNF probe and also the extreme deformation condition. We again observe a variation that approximates a cosinusoidal curve with peak-to-peak amplitude of ± 0.75 mm which is due to gravitional deformation. We also observe an offset between the two cases of roughly 0.25 mm and this may be attributed to non-intersection of the θ and ϕ axes and can be corrected for by shimming of the θ stage [3, p. 422]. Inspecting the curves representing the θ = ±30° and ±60° cases we see similar structural responses.

Figure 6 shows θ' angular error in degrees as a function of variable ϕ for six distinct values of variable θ. The curve for θ = 0° is omitted since this case represents the polar case and the conversion from laser tracker Cartesian to desired spherical coordinates is unstable at the polar location. The two curves depicting θ = ±90° (solid and dashed curves with ■ symbol) again represent the equatorial motion of the SNF probe and also the extreme deformation condition. We observe a variation that approximates a cosinusoidal curve with peak-to-peak amplitude of roughly ± 0.1°. A 180° lateral shift of the two curves was expected due to the reversal of the gravity vector for positive versus negative θ angles. However, a closer to 90° lateral shift of the two curves is noted and may be due to the complex flexure of the scanner structure. The curves depicting θ = ±60° & ± 30° display reduced structural deformation with a peak-to-peak amplitude variation of roughly ± 0.07°.

Figure 7 depicts ϕ' angular error in degrees as a function of variable ϕ for six distinct values of variable θ. The curve for θ = 0° is again omitted. The two curves depicting θ = ±90° (solid and dashed curves with ■ symbol) represent the extreme deformation condition. We again observe a variation that approximates a cosinusoidal curve with peak-to-peak amplitude of roughly ± 0.1° (for each curve) which is due to gravitational deformation.

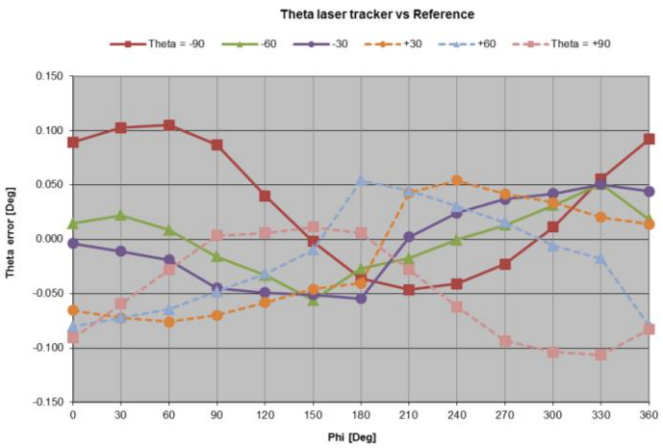

Figure 6. Strucural laser tracker measurement showing θ error as a function of ϕ variable. Curves represent discrete values of θ variable.

An expected 180° lateral shift of the two curves is noted due to the reversal of the gravity vector for positive versus negative θ angles. The curves depicting θ = ±60° & ± 30° again display reduced structural deformation with a peak-to-peak amplitude variation of roughly ± 0.05°.

It is worthwhile to also note that the average error offset between the two curves depicting θ = ±90° is roughly 0.2° and this could possibly be removed by reducing axis non-intersection. A similar (but reduced) offset can be observed for the θ = ±60° & ± 30° cases.

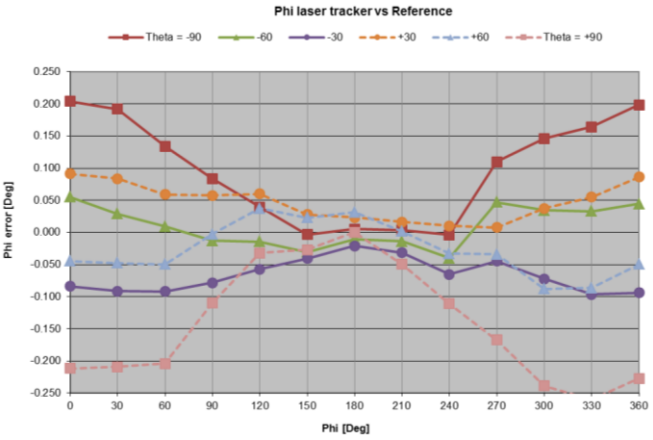

Figure 7. Strucural measurement using a laser tracker, showing ϕ error as a function of ϕ variable. Curves represent discrete values of θ variable.

IV. SCANNER STRUCTURAL CORRECTION

The SNF probe location errors describe in Section III are known once measured and can be corrected for, to within bounds determined by positioner repeatability limits. The data shown above are open loop values (i.e. no encoder feedback) and although absolute angular positioning can be improved (and backlash detected and corrected for) by adding axial

encoders, this will not detect or allow for the correction of any gravitational deformation of the articulating arms. A solution that is feasible to implement is to construct an error map (based on laser tracker measurements taken at the tip of the SNF probe) for all three variables as a function of angles $0° \leq \phi \leq 360°$ & $-180° \leq \theta \leq 180°$ (the redundant sphere) and to simply introduced an angular correction when locating the SNF probe. The angular data presented in Figures 6 & 7 show that these functions are not rapidly varying and linear interpolation for a reasonably coarse laser tracker grid is feasible. This type of correction can be implemented and successfully reduce typical angular errors by up to an estimated factor of 5. This correction can be achieved using the NSI-SC-5915 Panther Motion Controller (PMC) which allows for simultaneous control of up to 8 motion stages. This controller allows for dynamic on-the-fly cross axis correction based on laser tracker generated error grids as acquired for this scanner.

Correction for errors in *r'* is not possible through hardware in the absence of a linear radial actuator. An alternative is to consider R-correction as described in [2]. Results obtained for *r'* as a function of (θ, ϕ) are depicted below in Figure 8. (Note that this color map is obtained through laser tracker measurement and extrapolation to approximate deformation in regions that cannot be directly measured.) By subtracting the fixed value of *r*, the radial distance error can be obtained and from this an electrical phase correction calculated for each SNF probe position. This phase correction can then be applied to the measured SNF data as a first order correction term to remove the phase impact of the radial structural variation.

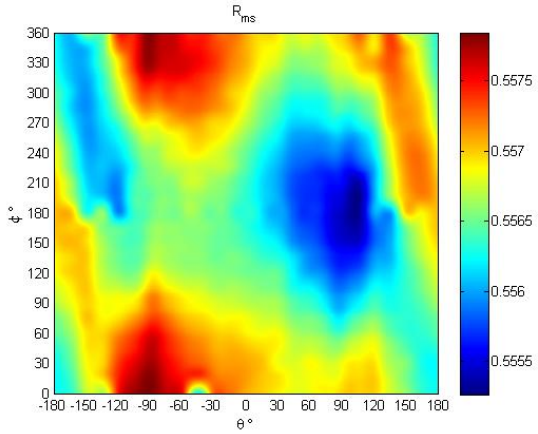

Figure 8. Scanner radius *r'* map shown as a function of (θ, ϕ). The radius variation observed is ±1 mm.

Figure 9 shows a typical SNF phase map for a single polarization component before and after correction for a test case at 140 GHz. In this instance the phase correction spans a range of almost 200° of electrical phase and is therefore significant. The success of this R-correction was demonstrated in [2].

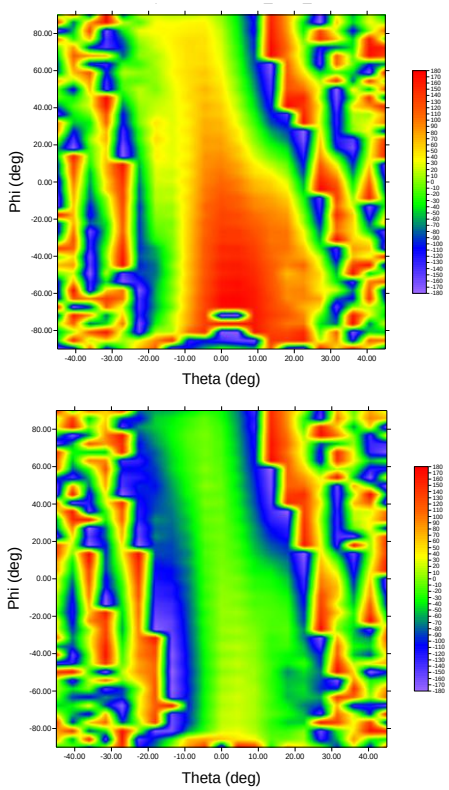

Figure 9. SNF phase distribution for a single polarization component pre R-correction (top) and post R-correction (bottom) at 140 GHz.

V. Structure Imposed High Frequency Limitations

Based on the structural deformation data presented in Section IV we can establish a feasible high frequency limit for SNF testing using this scanner structure. Based on the maximum uncorrected angular uncertainty of ±0.2° (worst case) our expected minimum SNF sampling interval is 2°, which corresponds to an AUT of maximum directivity (*Dir)* value of roughly 35 dBi. (In [4] it was shown that a random error of less than 1/10 of the sampling interval is required to achieve far-field error levels of < –30 dB.)

For measuring antennas of higher directivity, structural correction will be needed in order to reduce the ±0.2° angular uncertainty. Should one be able to achieve an uncertainty of ±0.04° (a factor 5 improvement using the PMC) our minimum SNF sampling interval is 0.4°, which corresponds to an AUT of maximum *Dir* of roughly 50 dBi.

For SNF testing a more critical aspect to control is a constant radius during measurement. In Section III we saw a radial distance variation of roughly ±1 mm peak-to-peak, which represents approximately ±0.5λ at 140 GHz. This can be corrected for using R-correction, but requires structural and RF stability. To date successful measurements have been taken up to this frequency and R-correction applied. Should R-correction prove to be unfeasible for higher frequencies due to a lack of

measurement repeatability, this may represent the upper frequency of operation for SNF testing for this scanner.

In [2] it was established that the system can be used for far-field testing if the 500 mm probe to AUT separation distance is sufficient to satisfy the far-field criterion. It was also shown that this limitation becomes less restrictive for increasing frequency. In Figure 10 directivity curves are shown for aperture efficiency values of 50%, 75% and 100% and the curve illustrates that for a fixed FF distance, higher gain antennas can be measured as the frequency is increased.

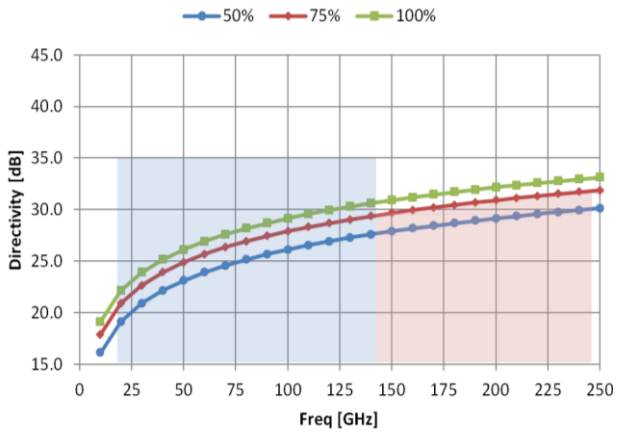

Figure 10. Maximum antenna directivity that can be tested in the far-field mode at a 500 mm distance. Directivity shown in dB as a function of frequency for 50%, 75% and 100% aperture efficiency [2]. Shaded area below 140 GHz represents possible SNF test zone, up to max directivity of 35 dBi. Shaded area below 75% aperture efficiency curve extending to 250 GHz represents FF test zone. The 250 GHz upper limit is selected for convenience and the actual limit will be determined by RF sub-system limitations.

The shaded area extending up to 35 dBi and below 140 GHz in Figure 10, represent the region of possible SNF test cases for the system. The shaded area extending up to the 75% aperture efficiency curve (selected here as a typical/realistic value) and below 250 GHz in Figure 10, represent the region of possible FF test cases for the system. This clearly shows that the excluded region would be for all antennas with directivity greater than 35 dBi up to 140 GHz and for antennas with directivity greater than the far-field curves depict in Figure 10, for frequencies greater than 140 GHz.

VI. Conclusions

We described and quantified the structural deformation of an articulating arm scanner designed for use at mm-wave frequencies. Based on this information we have previously shown [2] that antennas with directivity values of up to 35 dBi can be measured in SNF mode with a scanner of this design. This is based on the fact that angular uncertainty sensitivity is driven by SNF sampling density and not frequency.

The critical SNF parameter that is frequency sensitive is radial distance variation and it was shown before that SNF system sensitivity to large (> 90° phase) radial error is high [2]. Laser tracker dimensional measurements can be used to do R-correction to compensate for this and success has recently been demonstrated up to 140 GHz, raising the prior reported limit of 110 GHz. The scanner under consideration displays a radial distance variation of ±1 mm peak-to-peak, which represents roughly ±0.5λ at 140 GHz.

Far-field testing for this system is restricted by the fixed 500 mm probe to AUT separation distance. This finite distance becomes less impeding as frequency increases [2] and it is shown here that testing at frequencies greater than 140 GHz in FF mode is possible as long as the AUT directivity does not exceed the limits shown. The specific region of exclusion is depicted and represents what we believe to be the current commercial limit of what can be achieved with SNF testing at these challenging frequencies.

Acknowledgement

The authors would like to acknowledge Dan Swan, Karl Haner and Pat Pelland for their contributions towards this work.

References

[1] D. Janse van Rensburg and S. Gregson, “Parametric Study of Probe Positioning Errors in Articulated Spherical Near-field Test Systems for mm-Wave Applications”, IEEE Conference on Antenna Measurements & Applications, Antibes Juan-les-Pins (France), 16-19th Nov. 2014.

[2] D. Janse van Rensburg , “Factors limiting the upper frequency of mm-wave spherical near-field test systems”, EUCAP 2015, Lisbon (Portugal), 12 – 17 April 2015.

[3] C. Parini, S. Gregson, J. McCormick & D. Janse van Rensburg, Theory and Practice of Modern Antenna Range Measurements, IET, London, 2014. ISBN 978-1-84919-560-7.

[4] D. Janse van Rensburg, J. Wynne, “Parametric Study of Probe Positioning Errors in Spherical Near-field Test Systems for mm-Wave Applications”, IEEE APS/URSI, Conference Chicago, 2012.